Signature of heavy sterile neutrinos at CEPC

Wei Liao and Xiao-Hong Wu

Institute of Modern Physics, School of Science, East China University of Science and Technology, Meilong Road 130, Shanghai 200237, China

(Received 31 October 2017; published 5 March 2018)

We study the production of heavy sterile neutrino N, $e^+e^- \to N\nu(\bar{\nu})$, at the Circular Electron Positron Collider (CEPC) and its ljj signal in its decay to three charged fermions. We study background events for this process which are mainly events coming from W pair production. We study the production of a single heavy sterile neutrino and the sensitivity of CEPC to the mixing of the sterile neutrino with active neutrinos. We study the production of two degenerate heavy sterile neutrinos in a low energy seesaw model by taking into account the constraints on mixings of sterile neutrinos from the neutrinoless double β decay experiment and the masses and mixings of active neutrinos. We show that CEPC under proposal has a good sensitivity to the mixing of sterile neutrinos with active neutrinos for a mass of a sterile neutrino around 100 GeV.

DOI: 10.1103/PhysRevD.97.055005

I. INTRODUCTION

The establishment of neutrino oscillation and tiny masses of active neutrinos in past decades has raised strong hope that new physics beyond the Standard Model (SM) may exist in the leptonic sector of elementary particles. The seesaw mechanism [1], as a simple and straightforward extension of neutrinos in the SM, works as a very good mechanism to explain the tiny masses of active neutrinos and is a very good candidate for physics beyond the SM. In the seesaw mechanism, several right-handed neutrinos uncharged under the SM gauge groups, hence a type of sterile neutrino, are introduced with heavy Majorana-type masses which violate lepton number. The tiny masses of active neutrinos are understood in the low energy scale as the lepton number violating remnant of the Majorana-type masses of heavy right-handed neutrinos.

Although seesaw-type models are quite interesting models of physics beyond the SM and have fruitful implications, there are very few clues regarding the mass scale of right-handed neutrinos. In particular, the mass scale of right-handed neutrinos can be much higher than the electroweak scale. Therefore, it is very hard to test models of such type in experiments if such a hierarchy between the mass scale of right-handed neutrinos and the electroweak scale indeed exists. For this reason, a low energy scale seesaw type model [2], which has right-handed neutrinos at or below the electroweak scale, is quite interesting since it is possible to test it in experiments. There are several interesting properties of this low energy seesaw model. For example, one of the right-handed neutrinos can be of keV scale and serves as a good candidate for warm dark matter (WDM) in the universe. Two other right-handed neutrinos in the model are at GeV or 100 GeV scale and are sufficient to generate tiny masses and mixings of active neutrinos measured in neutrino oscillation experiments.

Another interesting property in this type of low energy seesaw model is that the Yukawa couplings of right-handed neutrinos with SM neutrinos can be quite large while still giving rise to masses and mixing of active neutrinos consistent with the experimental data in neutrino oscillation and the constraint from neutrinoless double β ($0\nu\beta\beta$) experiment [3,4], in particular when two heavy right-handed neutrinos are degenerate or quasidegenerate. Consequently, the mixings of right-handed neutrinos with active neutrinos in the SM can be quite large when the masses of right-handed neutrinos are at GeV to 100 GeV scale. This scenario apparently offers great opportunities to search for seesaw-type models of physics beyond the SM in collider experiments.

Experimentally, the single heavy neutrino has been searched for by the L3 collaboration at LEP through the $N \to eW$ channel [5,6]. A stringent constraint on $|R_{eN}|^2$ has been set for a mass region from 80 GeV to 205 GeV. Some efforts have been made to study the production and signature of heavy neutrinos in e^+e^- or e^-e^- collision processes with both pair and single heavy neutrino productions, and various neutrino decay chains, lW, νZ and νH [7–26]; for a review, see [24]. Currently, new electron-positron colliders, such as CEPC, Future Circular Collider

(FCC), and International Linear Collider (ILC), are under proposal. With these colliders, heavy sterile neutrinos can be probed to a larger mass range and with better sensitivity on the active-sterile mixing R_{lN}. Recently, single heavy neutrino production modes $N\nu$ and $Ne^{\pm}W^{\mp}$ at ILC with center of mass energy 350 GeV and 500 GeV have been investigated in [21]. A search of long-lived heavy neutrinos with displaced vertices at CEPC, FCC, and ILC has been presented in Ref. [23]. In our work, we present a detailed study of $e^+e^- \to N\nu$ with charged current neutrino decay mode $N \to lW$ at CEPC with center of mass energy $\sqrt{s} = 240$ GeV.

In the present article, we are motivated by such kinds of possibility and study the signature of this type of right-handed neutrino (or sterile neutrino) of 100 GeV masses at CEPC [27], a collider under proposal. In the next section, we will make a quick review of the low energy seesaw model and describe some basic properties of this model. Then we discuss the collider signatures of a single sterile neutrino of a mass around 100 GeV. For simplicity, we simplify our discussion of collider signature using a single sterile neutrino. We will show that this simplification can be taken as a good simplification for later discussion. Then we come to signatures of the low energy seesaw model by including detailed constraints on the masses and mixings of right-handed neutrinos. We conclude in the last section.

II. GEV SCALE STERILE NEUTRINO AND LOW ENERGY SEESAW MODEL

One of major differences between the case of a single GeV scale sterile neutrino and the low energy seesaw-type model of GeV scale sterile neutrinos is that for the former the mixings of sterile neutrinos with active neutrino are strongly constrained by the $0\nu\beta\beta$ decay experiment [28], while for the latter the $0\nu\beta\beta$ constraint can be quite weak and the mixings can be quite large [3].

In the presence of one or several sterile neutrinos, active neutrinos in the flavor base $\nu_l (l = e, \mu, \tau)$ are a mixture of the light neutrinos in mass eigenstates $\nu_i (i = 1, 2, 3)$ and heavy sterile neutrinos in mass eigenstates N_j,

$$\nu_l = \sum_i U_{li}\nu_i + \sum_j R_{lN_j} N_j, \tag{1}$$

where U_{lj} is the Pontecorvo-Maki-Nakagawa-Sakata (PMNS) mixing matrix, and R_{lN_j} is the matrix element mixing ν_l with heavy neutrinos N_j. For small enough $|R_{lN_j}|$, mixing matrix U can be considered as approximately unitary. Apparently, ν_i and N_j can all contribute, in a virtual intermediate state, to the $0\nu\beta\beta$ decay. It is not hard to see that the contribution of a single GeV scale sterile neutrino to the amplitude of the $0\nu\beta\beta$ decay is proportional to R^2_{eN}/M_N. The mixing R_{eN} in this case is constrained to be $|R_{eN}|^2 \lesssim 10^{-5}$ [28], unless there are other particles or mechanisms at hand to ease the constraint.

In the low energy seesaw type model, at least two heavy sterile neutrinos (right-handed neutrinos) are needed to obtain the correct masses and flavor mixings of active neutrinos [3]. In this case, the mixing matrix R is $R = Yv(M^*)^{-1}$ where Y is the Yukawa coupling of neutrinos, v the vacuum expectation value in the SM, and M the Majorana mass matrix of sterile neutrinos which can be taken to be real and diagonal in a convenient base. The matrix M is a 2×2 matrix if considering two heavy sterile neutrinos and a 3×3 matrix if considering three heavy sterile neutrinos.

A nice feature in the seesaw model is that mixing R is related to m_ν, the mass matrix of active neutrinos responsible for the neutrino oscillation phenomena,

$$(m_\nu)_{ll'} = -v^2 \sum_i Y^*_{li} Y^*_{l'i} M_i^{-1} = -\sum_i M_i R^*_{lN_i} R^*_{l'N_i}, \tag{2}$$

where M_i is the eigenvalue of matrix M, that is, we have chosen a base in which M is diagonal. One can see that if a strong cancellation happens between contributions of different sterile neutrinos in (2), a mass matrix m_ν at 10^{-3}–10^{-2} eV scale can be generated for M_i of 100 GeV scale and for pretty large $|R_{lN_i}|$.

Using mixing matrix R, contributions of heavy sterile neutrinos to the amplitude of $0\nu\beta\beta$ decay can be parametrized as follows:

$$\mathcal{A} = F \sum_i R^2_{eN_i} M_i^{-1}, \tag{3}$$

where F is an overall factor. For two heavy sterile neutrinos N_1 and N_2, (3) can be rewritten as

$$\mathcal{A} = \frac{F}{M_1^2}(R^2_{eN_1} M_1 + R^2_{eN_2} M_2) + F M_2 R^2_{eN_2}\left(\frac{1}{M_2^2} - \frac{1}{M_1^2}\right), \tag{4}$$

where M_1 and M_2 are the masses of N_1 and N_2, respectively. By taking $M_{1,2}$ to be real in a convenient base, one can see in (2) and (4) that the first term in (4) is of order 10^{-3}–10^{-2} eV$/M_1^2$ and can be neglected. The second term in (4) can be arbitrarily small if N_1 and N_2 are quasidegenerate or degenerate. One can see clearly that the constraint from $0\nu\beta\beta$ decay is no longer strong for two quasidegenerate heavy sterile neutrinos, which is exactly what happens in the low energy seesaw model.

A straightforward consequence of the above discussion about (4) and (2) and the degeneracy of N_1 and N_2 is that for sterile neutrinos of GeV to 100 GeV mass, a large value of $|R_{eN_i}|^2$ is only possible when

$$R^2_{eN_1} = -R^2_{eN_2}, \quad \text{or} \quad R_{eN_1} = \pm i R_{eN_2}. \tag{5}$$

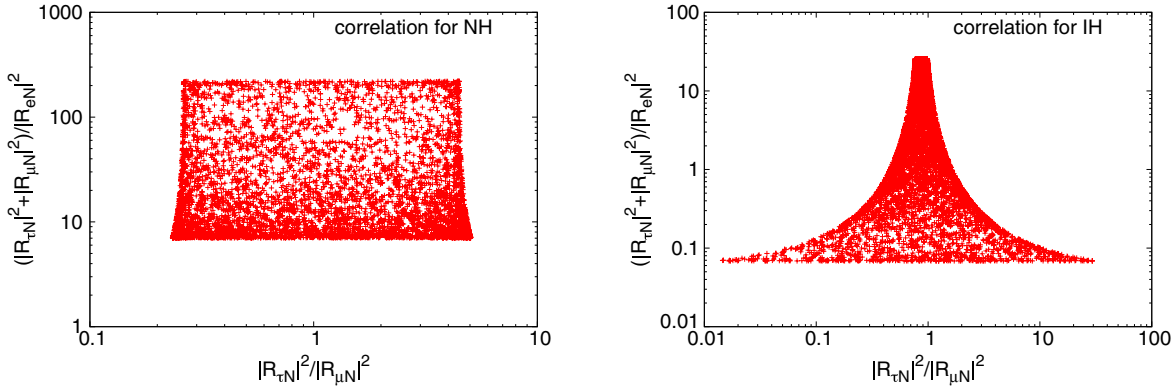

FIG. 1. $(|R_{\tau N_1}|^2 + |R_{\mu N_1}|^2)/|R_{eN_1}|^2$ versus $|R_{\tau N_1}|^2/|R_{\mu N_1}|^2$ for NH and IH, respectively.

Equation (5) is one of the major relations to be used in later analysis for discussing the collider signal of the low energy seesaw model.

Relations among $R_{\mu N_i}$ and $R_{\tau N_i}$ can also be addressed similarly. Using solutions presented for two heavy sterile neutrinos in [3], one can find that R_{lN_i} can be expressed as

$$R_{lN_1} = \frac{1}{2} e^{\mp ix+|y|}(U_{l2} m_2^{1/2} e^{-i\phi_2/2} \mp i U_{l3} m_3^{1/2} e^{-i\phi_3/2}) \times (M_1^*)^{-1/2}, \qquad R_{lN_2} = \pm i R_{lN_1}, \tag{6}$$

for normal hierarchy (NH) of neutrino masses, and

$$R_{lN_1} = \frac{1}{2} e^{\mp ix+|y|}(U_{l1} m_1^{1/2} e^{-i\phi_1/2} \mp i U_{l2} m_2^{1/2} e^{-i\phi_2/2}) \times (M_1^*)^{-1/2}, \qquad R_{lN_2} = \pm i R_{lN_1}, \tag{7}$$

for inverted hierarchy (IH) of neutrino masses. $m_{1,2,3}$ are real masses of $\nu_{1,2,3}$, and $\phi_{1,2,3}$ the associated Majorana phases in diagonal form of m_ν. For NH, $m_1 = 0$, $m_2 = \sqrt{\Delta m_{21}^2}$, $m_3 = \sqrt{|\Delta m_{32}^2| + \Delta m_{21}^2}$. For IH, $m_3 = 0$, $m_1 = \sqrt{|\Delta m_{32}^2| - \Delta m_{21}^2}$, $m_2 = \sqrt{|\Delta m_{32}^2|}$. x and y are two real free parameters to parametrize the mass matrix. Equations (6) and (7) are valid for large values of y, i.e., for the case that cancellation in (4) is needed to satisfy the $0\nu\beta\beta$ constraint.

One can see in (6) and (7) that $|R_{lN_2}|^2 = |R_{lN_1}|^2$ is valid for all flavors of neutrinos $\nu_{l=\tau,\mu,e}$, not just for $l = e$. This is one of the major properties of the low energy seesaw model if allowing large mixing of sterile neutrinos with active neutrinos. Using (6) and (7), one can also show the correlation of $|R_{lN_1}|^2$ by varying the free Dirac phase in matrix U and the Majorana phases ϕ_i. In Fig. 1 we plot the correlation of $(|R_{\tau N_1}|^2 + |R_{\mu N_1}|^2)/|R_{eN_1}|^2$ versus $|R_{\tau N_1}|^2/|R_{\mu N_1}|^2$. In our computation we use [29]

$$\sin^2 2\theta_{12} = 0.846, \qquad \sin^2 2\theta_{23} = 0.999, \qquad \sin^2 2\theta_{13} = 0.093, \tag{8}$$

and

$$\Delta m_{21}^2 = 7.53 \times 10^{-5}\ \text{eV}^2, \quad |\Delta m_{32}^2| = 2.48 \times 10^{-3}\ \text{eV}^2. \tag{9}$$

For Δm_{32}^2 we have averaged two fit values for NH and IH [29]. One can see in these plots that the mixings of sterile neutrinos with ν_τ and ν_μ together are always stronger than the mixing with ν_e for NH. For IH, $|R_{\tau N_1}|^2 + |R_{\mu N_1}|^2$ can be larger than or smaller than $|R_{eN_1}|^2$. On the other hand, the ratio between $|R_{\tau N_1}|^2$ and $|R_{\mu N_1}|^2$ can be larger than or smaller than one for both NH and IH.

From the above discussions, one can see that a major implication of a low energy seesaw type model with two GeV scale sterile neutrinos and large mixings with active neutrinos is the relation of mixings, such as $|R_{lN_1}|^2 = |R_{lN_2}|^2$ and the correlation shown in Fig. 1. For discussion of collider signatures in this low energy seesaw model, one should take these relations into account. However, as a first step towards this goal, we can discuss the signature of a single sterile neutrino with a mass at around 100 GeV. The signature of the low energy seesaw model can be obtained by extending the discussion for a single sterile neutrino to two sterile neutrinos and taking into account these relations among mixings described above. A further advantage of first discussing a single sterile neutrino is that the case of a single sterile neutrino may also be valid if other particle or mechanisms, e.g., some scalar particles and Type-II seesaw mechanism, are introduced. So a discussion on the collider signature of a single heavy sterile neutrino is of interest in and of itself. Needless to say, discussing the signature of a heavy sterile neutrino together with signature of other particles, e.g., scalar particles in type-II seesaw mechanism, is also of interest. In the present article, we are not going to elaborate on this topic. In the next section, we discuss the signature of a single sterile neutrino with a mass around 100 GeV at CEPC. We come back to the signature of the low energy seesaw model in later sections. For previous works on the signature of heavy sterile neutrinos on e^+e^-

colliders, one can see a review in [24]. The present work gives a discussion on the signature of heavy sterile neutrino on CEPC within the framework of the low energy seesaw model and differs from the previous works in these aspect.

The mixings of sterile neutrinos with active neutrinos are also subject to the indirect constraints from tests of lepton universality, lepton flavor violation processes, and electroweak precision measurements [30–35]. For the heavy neutrino masses of order of 100 GeV, $|R_{eN}|^2$, $|R_{\mu N}|^2$, and $|R_{\tau N}|^2$ are constrained to be $\mathcal{O}(10^{-3})$ mainly by the lepton flavor conserved decays of charged leptons, mesons, W, and Z. The combination $|R^*_{\mu N}R_{eN}|$ is stringently constrained to be order of 10^{-5} from the upper bounds of $\mu \to e\gamma$ and $\mu - e$ conversion. These indirect constraints are complementary to the probing of heavy sterile neutrinos at e^+e^- colliders. As will be shown in later sections, CEPC will probe $|R_{lN}|^2$ to 10^{-5}–10^{-6} and will have a better sensitivity than these indirect constraints at present.

III. PRODUCTION AND DECAY OF A HEAVY STERILE NEUTRINO

In this section, we discuss the production of a single heavy sterile neutrino at CEPC and its decay. CEPC under proposal plans to run electron-positron collision at a center of mass energy around 240 GeV and aims at obtaining an integrated luminosity up to 5 ab^{-1} with two interaction points and ten years of operation.

The Feynman diagrams of the production of a heavy Majorana-type sterile neutrino, N, are shown in Fig. 2. For simplicity, the heavy neutrino index j will be suppressed in discussion for a single heavy sterile neutrino. The leading contribution to N production is the process $e^+e^- \to N\nu_l(\bar{\nu}_l)$, the SM process $e^+e^- \to \nu_l\bar{\nu}_l$ with ν_l or $\bar{\nu}_l$ replaced by N via its mixing with ν_l. Because of the Majorana nature of N, it can mix with both ν_l and $\bar{\nu}_l$ with the same strength of mixing and can be produced via both of these mixings. These two possibilities are shown in the left and right panels in Fig. 2. As one can see in the upper panels of Fig. 2, the production of N can be mediated by a Z boson in s-channel with all types of neutrinos $\nu_l(\bar{\nu}_l)$ in final state. N production can also be mediated by a W boson in t-channel with $\nu_e(\bar{\nu}_e)$ in final state, as can be seen in the lower panels in Fig. 2. For the same strength of mixings, the t-channel process has a cross section two order of magnitude larger than the s-channel process and hence has a better sensitivities for the mixing R_{eN}.

We calculate the tree-level $e^+e^- \to N\nu_l$ cross sections with MadGraph [36] and implement the heavy neutrino interactions in FeynRules [37] with the Universal FeynRules Output (UFO) [38] format for the model. The results are shown in Fig. 3. For a heavy neutrino of about 100 GeV, the production cross section of $\sigma/|R_{eN}|^2$ and $\sigma/|R_{\mu N}|^2$ can reach ∼60 pb and ∼0.8 pb for only a single R_{eN} mixing or $R_{\mu N}$ mixing, respectively.

Mixing of sterile neutrino N with active neutrinos can lead to decay of N. For m_N, the mass of N, much smaller than m_W, the mass of a W boson, the leading decays of N are tree-level three-body decays mediated by off-shell W or Z bosons. Some three-body decay channels of N are quite simple. For example, $N \to e^-\mu^+\nu_\mu$ is mediated by an off-shell W boson and is similar to $\mu \to \nu_\mu e\bar{\nu}_e$, the leptonic decay of μ, except with the presence of a mixing factor $|R_{eN}|^2$ in decay rate. Some decay channels, e.g., $N \to \nu_e e^- e^+$, can be mediated by both off-shell W and Z bosons. But it does not introduce complications in the decay rate. The results are presented in (A18)–(A24) in the Appendix.

For m_N much greater than m_W and m_Z, the leading decay of N are two-body decays, $N \to l^\pm W^\mp$ and $N \to \nu(\bar{\nu})Z$.

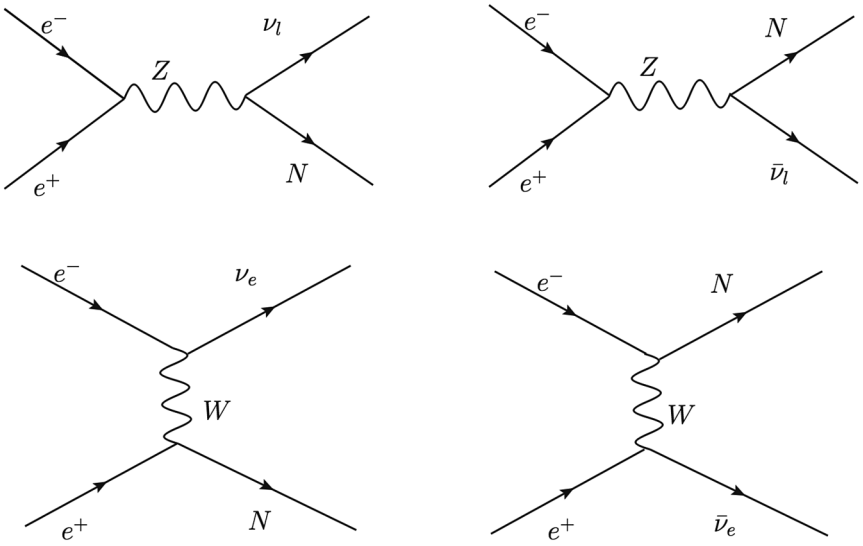

FIG. 2. Feynman diagrams.

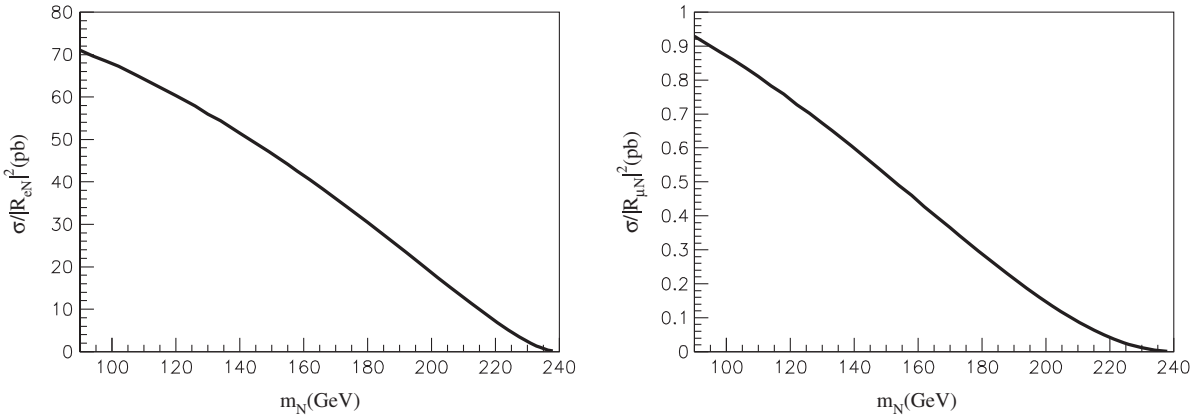

FIG. 3. $e^+e^- \to N\nu$ cross section at $\sqrt{s} = 240$ GeV with only a single R_{eN} mixing (left) and $R_{\mu N}$ mixing (right).

For m_N greater than m_H, the mass of the Higgs boson, N can also decay to H via $N \to \nu(\bar{\nu})H$. The partial decay widths of the heavy neutrino can be written as [3,21,39,40]

$$\Gamma(N \to l^- W^+) = \frac{g^2}{64\pi}|R_{lN}|^2 \frac{m_N^3}{m_W^2}(1-\mu_W)^2(1+2\mu_W) \tag{10}$$

$$\Gamma(N \to \nu Z) = \frac{g^2}{64\pi}|R_{lN}|^2 \frac{m_N^3}{m_W^2}(1-\mu_Z)^2(1+2\mu_Z) \tag{11}$$

$$\Gamma(N \to \nu H) = \frac{g^2}{64\pi}|R_{lN}|^2 \frac{m_N^3}{m_W^2}(1-\mu_H)^2 \tag{12}$$

with $\mu_i = m_i^2/m_N^2$ $(i = W, Z, H)$. W, Z, or H eventually decay to fermions. Hence, the decay rate to a specific three-body final state can be calculated using (10)–(12) and the branching ratio of W, Z, or H to a specific fermion pair. For example, $\Gamma(N \to e^-\mu^+\nu_\mu)$ is obtained using $\Gamma(N \to e^- W^+)$ and $\mathrm{Br}(W \to \mu^+\nu_\mu)$ as $\Gamma(N \to e^-\mu^+\nu_\mu) = \Gamma(N \to e^- W^+) \times \mathrm{Br}(W^+ \to \mu^+\nu_\mu)$, where $\mathrm{Br}(W^+ \to \mu^+\nu_\mu)$ is the branching ratio of $W^+ \to \mu^+\nu_\mu$ decay.

For more general values of m_N, in particular for $m_N \approx m_{W,Z,H}$, the above formulas are not good approximations. Decay rate in more general cases can be calculated by carefully including the propagators of W, Z, and H bosons into calculation. The four-momentum of the mediated boson can be on-shell for general cases. We take this fact into account and calculate the tree-level decay rate of N decays with three fermions in final state. In the Appendix, we present in detail the results of our calculations. One can see that for most cases the decay rate can be obtained as an analytic function of m_N and the masses and widths of bosons. The most complicated case appears for $N \to l^- l^+ \nu_l$ and $N \to l^- l^+ \bar{\nu}_l$ channels for which W and Z bosons can all mediate. For this particular process, a function F_S, shown in (A5) and (A15), appears, which cannot be obtained as an explicit analytic function of m_N and the boson masses. In our analysis we compute F_S numerically.

As an example, we compare in Fig. 4 the result computed using an analytic formula (A3) with known results in the low energy region $m_N \ll m_W$ and in the high energy limit $m_N > m_W$. $\Gamma(N \to e^- W^+)$ is calculated using (10). $\mathrm{Br}(W^+ \to \mu^+\nu_\mu)$ is taken as $\mathrm{Br} = 0.108$ [29]. We can see that in the low energy limit the decay rate agrees with the expected result of tree-level three-body decay. In the high energy limit it agrees with the expectation that it is dominated by the on-shell $N \to e^- W^+$ decay with a subsequent $W^+ \to \mu^+\nu_\mu$ decay. In the region around m_W, (A3) gives a smooth transition from low energy behavior to high energy behavior. As a comparison, the result calculated using the two body decay $N \to e^- W^+$ drops down to zero as m_N approaches m_W from above and is certainly not correct at around the threshold. The result given by (A3) takes into account the contribution of the off-shell boson and removes the ill behavior at around $m_N \sim m_W$. The plot demonstrates that the results presented in the Appendix are

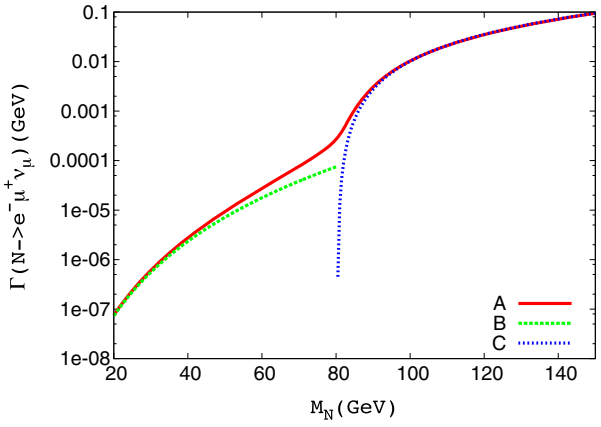

FIG. 4. Decay rate of $N \to e^-\mu^+\nu_\mu$ versus m_N with $|R_{eN}|^2 = 1$. Line A: calculated using (A3); Line B: calculated using $\Gamma = G_F^2 m_N^5/(192\pi^3)$ in (A18) up to $m_N < m_W$; Line C: calculated using $\Gamma = \Gamma(N \to e^- W^+)\mathrm{Br}(W^+ \to \mu^+\nu_\mu)$ with $m_N > m_W$.

better to use for studying the signals of the sterile neutrino. Tree-level three-body decay rates for general mass m_N, presented in the Appendix, are some of the new results of the present article.

IV. SIGNAL OF A HEAVY STERILE NEUTRINO AND BACKGROUND

In this section, we study the process

$$e^+e^- \to N\nu, \qquad N\bar{\nu} \to ljj\not{E}, \tag{13}$$

the signal of sterile neutrino N due to this process, and the associated background.

We simulate the signal and background events with MadGraph [36], and have done the showing and hadronization by using Pythia6 [41]. The results are passed through PGS4 [42] for fast detector simulation.

At CEPC with $\sqrt{s} = 240$ GeV, we adopt the basic cuts (BC) for lepton and jets to select the events,

$$p_T^l > 10 \text{ GeV}, \qquad |\eta^l| < 2.5, \qquad \Delta R_{ll} > 0.4, \tag{14}$$

$$p_T^j > 10 \text{ GeV}, \quad |\eta^j| < 2.5, \quad \Delta R_{jj} > 0.4, \quad \Delta R_{lj} > 0.4. \tag{15}$$

The main backgrounds for the process (13) are W pair production, $e^+e^- \to W^+W^-$, with one W decaying leptonically and the other W decaying hadronically, and single W production, which decays leptonically. In order to suppress the backgrounds, we set the selection cuts (SC) [21,39],

$$|M(l, \not{E}) - m_W| > 20 \text{ GeV}, \tag{16}$$

and

$$|M(l, j_1, j_2) - m_N| < 20 \quad \text{or} \quad 10 \text{ GeV}. \tag{17}$$

Cut (16) is used to exclude background events coming from the decay of on-shell W boson in the background processes. Cut (17) selects events coming from the decay of on-shell N and is used to increase the significance of signal-to-background ratio.

In Table I we show the efficiency of the cuts for both $l = e$ and $l = \mu$ channels. After adding the SC, the signals are survived, but the backgrounds drop several order of magnitude.

We define the significance s as

$$s = \frac{\mathcal{N}_s}{\sqrt{\mathcal{N}_s + \mathcal{N}_b}}, \tag{18}$$

where $\mathcal{N}_s$ and $\mathcal{N}_b$ are the event number of signal and background respectively. In Fig. 5 we plot the significance s versus m_N for $l = e$ with $R_{eN} = 0.015$ and $l = \mu$ with $R_{\mu N} = 0.1$, respectively. For the integrated luminosity of 100 fb^{-1}, a heavy neutral neutrino with mass in the range of 90 GeV $\le m_N \le$ 146 GeV for the mixing $R_{eN} = 0.015$ is promised to be discovered in the $l = e$ channel, and 90 GeV $\le m_N \le$ 150 GeV for the mixing $R_{\mu N} = 0.1$ is promised to be discovered in the $l = \mu$ channel. For the integrated luminosity of 5 ab^{-1}, the maximal values of heavy neutrino mass can be 235 GeV and 205 GeV for the $l = e$ and $l = \mu$ channel, respectively. One can see that there is a quick drop for heavy neutrinos with mass $\lesssim$100 GeV for both of $l = e$ and $l = \mu$. This is because for the decay of N of a mass $\lesssim$100 GeV, the lepton in $N \to lW \to ljj$, a decay chain with an almost on-shell W, does not have enough energy and the p_T of l cannot be large. This effect of cut on p_t of l can be seen in Table I C. In Fig. 5, one can also see that there is a small peak for a heavy neutrino with mass around 230 GeV. This is because of the cut $|M(l, \not{E}) - m_W| > 20$ GeV to the signal as shown in Table I E. Compared with the case of $m_N = 214$ GeV in Table I D, a heavier neutrino with mass of 230 GeV tends to move more slowly in the center of mass system of colliding

TABLE I. The cross sections (unit fb) of signal (upper line) after imposing various cuts (a, b, c, d, e) sequentially, the background (lower line) and the significance after cuts with integrated luminosity of 500 fb^{-1}. Cuts (a) $p_T^{j,l} > 1$ GeV, (b) $p_T^{j,l} > 10$ GeV, (c) $|M(l, \not{E}) - m_W| > 20$ GeV, (d) $|M(l, j_1, j_2) - m_N| < 20$ GeV, (e) $|M(l, j_1, j_2) - m_N| < 10$ GeV.

	parameters	+cuts (a)	+cuts (b)	+cuts (c)	+cuts (d)	+cuts (e)	significance
A	$m_N = 150$ GeV,	2.14	2.04	1.56	1.56	1.55	11.2
	$R_{\mu N} = 0.1$	2.31×10^3	2.20×10^3	52.4	16.3	8.05	
B	$m_N = 150$ GeV,	7.63	7.30	5.61	5.60	5.60	18.8
	$R_{eN} = 0.02$	2.52×10^3	2.37×10^3	0.195×10^3	76.6	38.8	
C	$m_N = 90$ GeV,	10.8	4.98	1.56	1.55	1.55	13.4
	$R_{eN} = 0.015$	2.52×10^3	2.37×10^3	0.195×10^3	16.8	5.14	
D	$m_N = 214$ GeV,	0.852	0.827	0.243	0.242	0.241	1.75
	$R_{eN} = 0.015$	2.52×10^3	2.37×10^3	0.195×10^3	24.9	9.26	
E	$m_N = 230$ GeV,	0.194	0.188	0.160	0.160	0.160	2.76
	$R_{eN} = 0.015$	2.54×10^3	2.39×10^3	0.197×10^3	4.14	1.49	

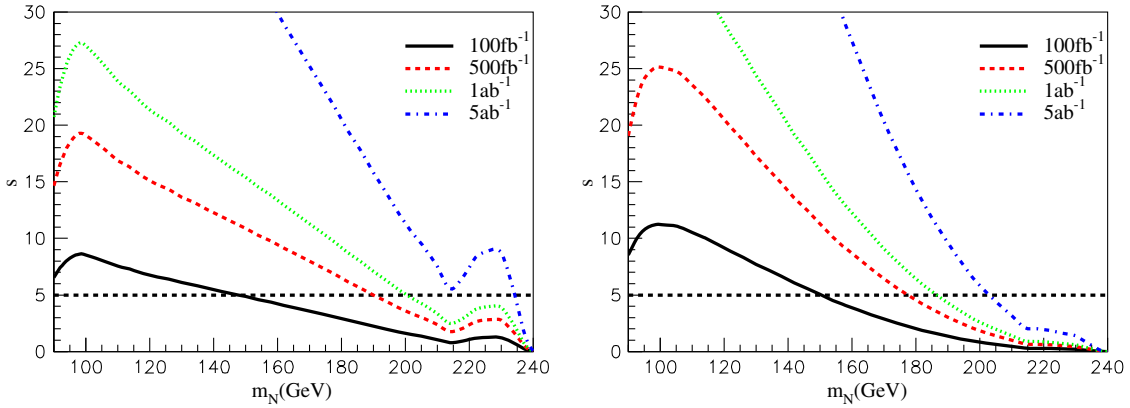

FIG. 5. The significance for $l = e$ (left) with $R_{eN} = 0.015$ and $l = \mu$ (right) with $R_{\mu N} = 0.1$. The curves in each plot from up to down correspond to the integrated luminosities 5 ab^{-1}, 1 ab^{-1}, 500 fb^{-1}, and 100 fb^{-1}.

e^+e^-, and it decays to a charged lepton which distributes more uniformly in all directions. More importantly, the light neutrino, produced together with the heavier sterile neutrino with a mass of 230 GeV, becomes quite soft (with an energy ≈9.8 GeV). Then, the invariant mass of the light neutrino and charged lepton $M(l, \not{E})$ will distribute more evenly. Consequently, the cut $|M(l, \not{E}) - m_W| > 20$ GeV does not hurt the signal as much as in the case of $m_N = 214$ GeV, as shown in Table I D and E. This can be verified if the cut (c) is changed to $|M(l, \not{E}) - m_W| > 10(30)$ GeV, the signal cross section is changed to 0.188 (0.103) fb, respectively. On the other hand, the background cross section reduces significantly with $m_N = 230$ GeV in Table I E after adding all the cuts.

In Fig. 6 we plot the potential of probing R_{lN} for a fixed significance $s = 5$ with the integrated luminosities 5 ab^{-1},

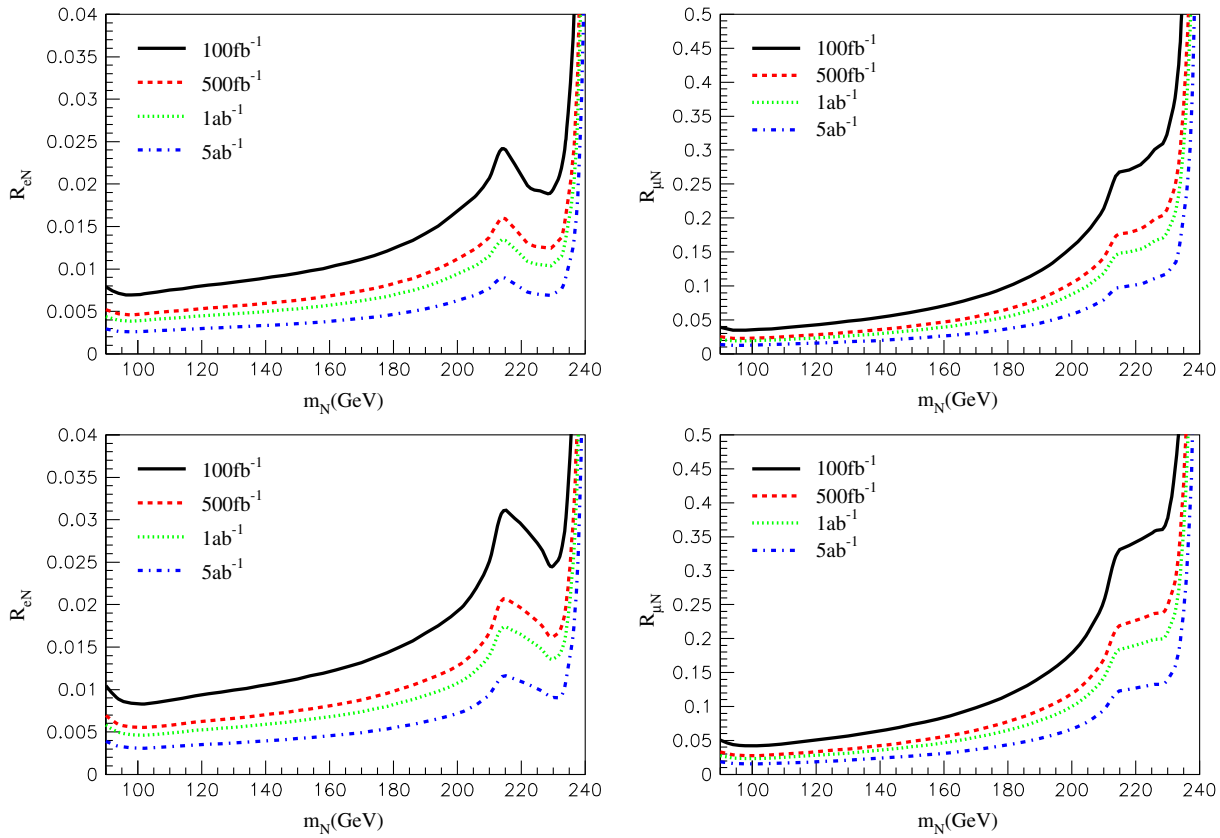

FIG. 6. Sensitivity to R_{lN} $(l = e, \mu)$ with significance $s = 5$. The upper plots are for SC $|M(l, j_1, j_2) - m_N| < 10$ GeV and the lower plots are for SC $|M(l, j_1, j_2) - m_N| < 20$ GeV. The curves in each plot from up to down correspond to integrated luminosities 100 fb^{-1}, 500 fb^{-1}, 1 ab^{-1}, and 5 ab^{-1}.

1 ab^{-1}, 500 fb^{-1}, and 100 fb^{-1} at CEPC. Using SC $|M(l,j_1,j_2)-m_N|<10$ GeV, in the $l=e$ channel, a heavy neutrino mass of 120 GeV with $R_{eN}=0.0080$ can be discovered for the integrated luminosities 100 fb^{-1}, and for 5 ab^{-1}, the mixing as low as $R_{eN}=0.0030$ for the same mass can be probed. In the $l=\mu$ channel, the heavy neutrino of the same mass with $R_{\mu N}=0.043$ can be discovered for 100 fb^{-1}, and $R_{\mu N}=0.016$ for 5 ab^{-1}. We can have similar results for SC $|M(l,j_1,j_2)-m_N|<20$ GeV, but the corresponding mixings are a little bigger.

V. SIGNAL OF LOW ENERGY SEESAW MODEL

In this section we discuss the signature of the low energy seesaw model with two heavy sterile neutrinos of mass around 100 GeV.

As discussed in previous section, in the case of large mixing of heavy sterile neutrinos with active neutrinos, not only the masses of these two sterile neutrinos are (quasi) degenerate but also the mixing has a simple relation $R_{lN_2}=\pm iR_{lN_1}$ as shown in (6) and (7). So the signature of the low energy seesaw model discussed here is just the double of the result presented for a single heavy sterile neutrino, except that we need to take into account the correlation of the mixing R_{lN} for different l in the low energy seesaw model, as shown in Fig. 1.

We calculate the signal of $e^+e^-\to\nu ljj$ events and the related background for $l=e$, μ, τ separately. Then we calculate the significance of $e^+e^-\to\nu ljj$ events for $l=e$, μ, τ separately. The total significance is defined as the square root of the sum of the squares of the significances of signals of $l=e$, $l=\mu$, and $l=\tau$, which we call $e+\mu+\tau$ significance. Similarly, we can define $e+\mu$ significance, which includes signals of $l=e$ and $l=\mu$. For simplicity, we assume 100% efficiency of the identification of the τ lepton. A realistic efficiency can be put into analysis without difficulty and would give rise to a result between the lines of $e+\mu+\tau$ significance and $e+\mu$ significance presented in figures below.

We plot the significance versus the mass of heavy neutrinos in Fig. 7 for NH and IH with parameters given in the caption and with integrated luminosity 500 fb^{-1} as an illustration. In the case of NH, we choose to have $|R_{\mu N}|$ about 10 times larger than $|R_{eN}|$ for $\delta_{\rm CP}=\pi/2$. $R_{\tau N}$ is of the same magnitude as $R_{\mu N}$, so the dominant decay channels are the μ and τ channels which dominate the total significance in the figure. For $\delta_{\rm CP}=-\pi/2$, $|R_{\mu N}|$ is of the same size of $|R_{\tau N}|$, but approximately 2 times larger than $|R_{eN}|$. Furthermore, the backgrounds for the μ and τ channels are several times smaller than the e channel. Thus, the μ and τ channels are still dominant in $e+\mu+\tau$ significance.

As can be seen in Fig. 7, in the case of NH, a heavy sterile neutrino with a mass less than about 152 GeV ($|R_{eN}|\sim0.0032$, $|R_{\mu N}|\sim|R_{\tau N}|\sim0.034$) can be discovered for $\delta_{\rm CP}=\pi/2$. For $\delta_{\rm CP}=-\pi/2$, a heavy sterile neutrino with a mass less than around 206 GeV ($|R_{eN}|\sim0.015$, $|R_{\mu N}|\sim|R_{\tau N}|\sim0.028$) can be discovered. As can be seen in the above example, the case with $\delta_{\rm CP}=-\pi/2$ has a larger $|R_{eN}|$. This larger value of $|R_{eN}|$ enhances the t-channel production process and gives rise to a larger production rate of heavy sterile neutrinos. Meanwhile, the μ or τ channel decay of N is still dominating over the e channel, so the significance increases a lot from the case of $\delta_{\rm CP}=\pi/2$ to the case of $\delta_{\rm CP}=-\pi/2$.

In the case of IH, we choose to have similar magnitude of $|R_{eN}|$, $|R_{\mu N}|$, and $|R_{\tau N}|$ for both cases of $\delta_{\rm CP}=\pi/2$ and $\delta_{\rm CP}=-\pi/2$. All three e, μ, and τ decay channels have comparable contributions to the total significance. For the Dirac phase of both cases of $\delta_{\rm CP}=\pi/2$ and $\delta_{\rm CP}=-\pi/2$, the magnitude of $|R_{eN}|$ has the same size, and so does $|R_{eN}|^2+|R_{\mu N}|^2+|R_{\tau N}|^2$. This leads to the same production rate of $e^+e^-\to\nu N$ and the same ljj decays of N for both

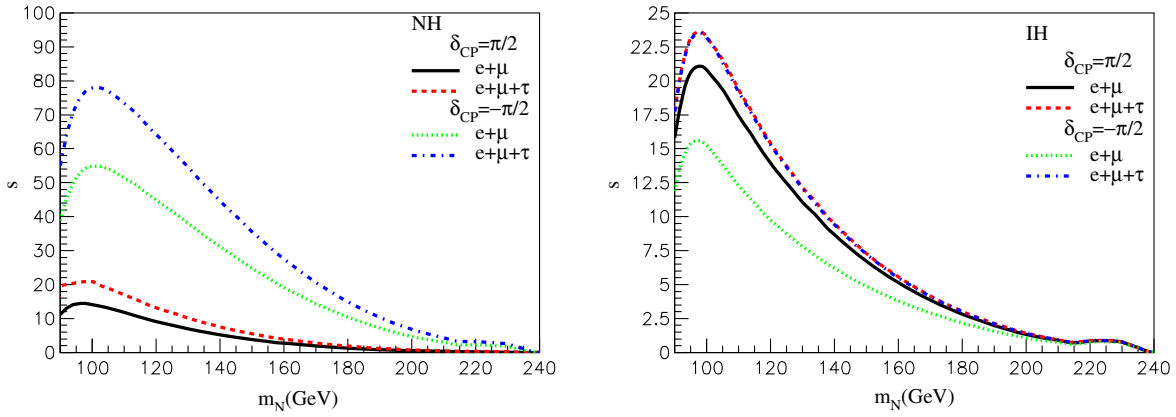

FIG. 7. The significance s vs m_N for NH (left) and IH (right) with integrated luminosity 500 fb^{-1}. We choose $e^y=5000$, $\delta_{\rm CP}=\pm\pi/2$, $\phi_1=\phi_2=\phi_3=0$ for NH (the largest eigenvalue of the matrix of neutrino Yukawa couplings defined in Ref. [32] is $0.00495\times\sqrt{m_N}$), and $e^y=1000$, $\delta_{\rm CP}=\pm\pi/2$, $\phi_1=\phi_2=\phi_3=0$ for IH (the largest eigenvalue of the matrix of neutrino Yukawa couplings is $0.00128\times\sqrt{m_N}$).

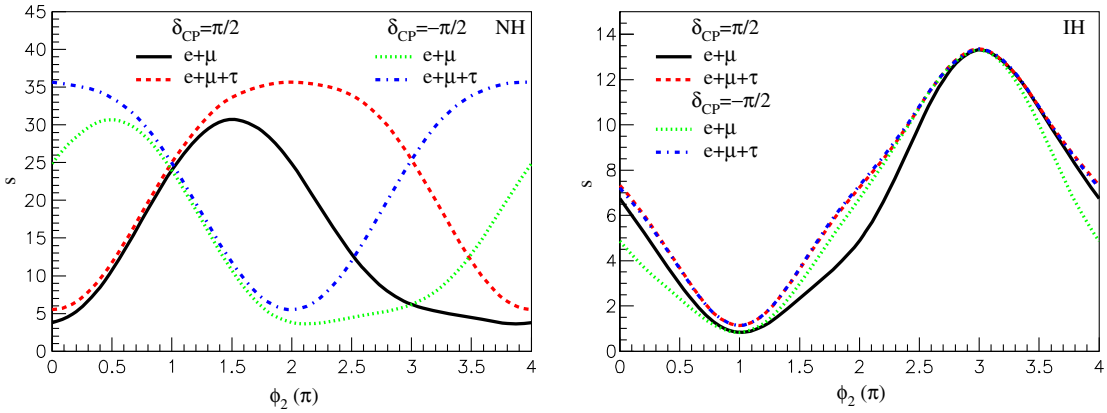

FIG. 8. The significance s vs ϕ_2 for NH (left) and IH (right) with integrated luminosity 500 fb^{-1} for a heavy neutrino mass of 150 GeV. We choose $e^y = 5000$, $\delta_{CP} = \pm\pi/2$, $\phi_1 = \phi_3 = 0$ for NH (the largest eigenvalue of the matrix of neutrino Yukawa couplings is 0.0606), and $e^y = 1000$, $\delta_{CP} = \pm\pi/2$, $\phi_1 = \phi_3 = 0$ for IH (the largest eigenvalue of the matrix of neutrino Yukawa couplings is 0.0156).

cases of $\delta_{CP} = \pi/2$ and $\delta_{CP} = -\pi/2$. So, the total $e + \mu + \tau$ significances are the same for both cases of $\delta_{CP} = \pi/2$ and $\delta_{CP} = -\pi/2$. However, there is a difference between the $e + \mu$ significances for these two cases. One can see in Fig. 7 that for IH a heavy neutrino with mass less than about 162 GeV can be discovered. The corresponding mixing parameters in the figure are $|R_{eN}| \sim 0.0086$, $|R_{\mu N}| \sim 0.0072$, $|R_{\tau N}| \sim 0.0051$ for $\delta_{CP} = \pi/2$, and $|R_{eN}| \sim 0.0086$, $|R_{\mu N}| \sim 0.0053$, $|R_{\tau N}| \sim 0.0071$ for $\delta_{CP} = -\pi/2$.

In Fig. 8, we also plot the total significance as a function of the Majorana phase ϕ_2 for a heavy neutrino mass of 150 GeV and integrated luminosity of 500 fb^{-1} for both NH and IH. The significance depends on both the Dirac phase of δ_{CP} and Majorana phase ϕ_2. In the case of NH with $\delta_{CP} = \pi/2$, there is a bump at $\phi_2 \sim 1.5\pi$ for $e + \mu$ significance. On the other hand, the bump is at around 2π for $e + \mu + \tau$ significance. This is because $|R_{eN}|^2/\sum |R_{lN}|^2$ increases as ϕ_2 increases from 0 to 2π, as can be seen in Fig. 9. Since $\sum |R_{lN}|^2$ is a constant when varying ϕ_2, as can

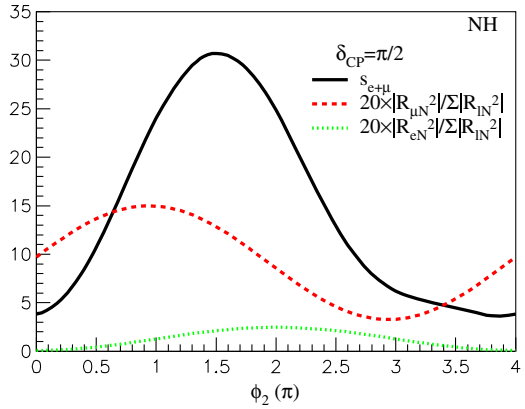

FIG. 9. The significance s vs ϕ_2 for NH with $\delta_{CP} = \pi/2$ with $e^y = 5000$, $\phi_1 = \phi_3 = 0$ (the largest eigenvalue of the matrix of neutrino Yukawa couplings is 0.0606), and integrated luminosity 500 fb^{-1}.

be easily checked using (6) and (7), $|R_{eN}|^2$ increases as ϕ_2 increases from 0 to 2π and peaks at $\phi_2 = 2\pi$. Consequently, the t-channel production process, the dominating production process, increases as ϕ_2 increases from 0 to 2π. This is why the plot of the $e + \mu + \tau$ significance peaks at $\phi_2 = 2\pi$ in the case of NH with $\delta_{CP} = \pi/2$. For the $e + \mu$ significance, it is dominated by the μjj events, as explained before. As ϕ_2 increases, $|R_{\mu N}|^2/\sum |R_{lN}|^2$ peaks at $\phi_2 \sim \pi$. For ϕ_2 larger than around π, the branching fraction of the $N \to \mu jj$ decay starts to decrease, which is compensated by the increase of the production cross section of $e^+e^- \to N\nu$. Then, the signature of μjj events will increase first and then decrease as ϕ_2 increases from π to 2π. This makes $e + \mu$ significance having a peak at a position less than 2π, as can seen in Fig. 8. Variation of significance in other cases can be similarly understood.

In Fig. 10, we present the significance as a function of heavy neutrino mass with integrated luminosity 5 ab^{-1}. In the case of NH, a heavy neutrino mass less than about 124 GeV ($|R_{eN}| \sim 0.0012$, $|R_{\mu N}| \sim |R_{\tau N}| \sim 0.013$) for $\delta_{CP} = \pi/2$, and 184 GeV ($|R_{eN}| \sim 0.0055$, $|R_{\mu N}| \sim |R_{\tau N}| \sim 0.010$) for $\delta_{CP} = -\pi/2$ can be discovered at CEPC. In the case of IH, a heavy neutrino mass less than about 130 GeV can be discovered. The corresponding mixing parameters are $|R_{eN}| \sim 0.0034$, $|R_{\mu N}| \sim 0.0028$, $|R_{\tau N}| \sim 0.0020$ for $\delta_{CP} = \pi/2$, and $|R_{eN}| \sim 0.0034$, $|R_{\mu N}| \sim 0.0021$, $|R_{\tau N}| \sim 0.0028$ for $\delta_{CP} = -\pi/2$.

In Fig. 11, we plot the potential of probing $|R_{\mu N}|$ for $e + \mu$ (or $e + \mu + \tau$) significance $s = 5$ with the integrated luminosities 5 ab^{-1}, 1 ab^{-1}, 500 fb^{-1} and 100 fb^{-1} at CEPC for different cases of NH and IH, and Dirac phase $\delta_{CP} = \pm\pi/2$. For each case, the ratio of $|R_{eN}|:|R_{\mu N}|:|R_{\tau N}|$ is fixed for the given Dirac phase and Majorana phases; therefore we only plot $|R_{\mu N}|$ for illustration. In the case of NH, the ratio of $|R_{eN}|:|R_{\mu N}|:|R_{\tau N}|$ is 0.0945:1:1.03 (0.537:1:1.02) for $\delta_{CP} = \pi/2$ ($\delta_{CP} = -\pi/2$). In the case of IH, the ratio of $|R_{eN}|:|R_{\mu N}|:|R_{\tau N}|$ is 1.19:1:0.709

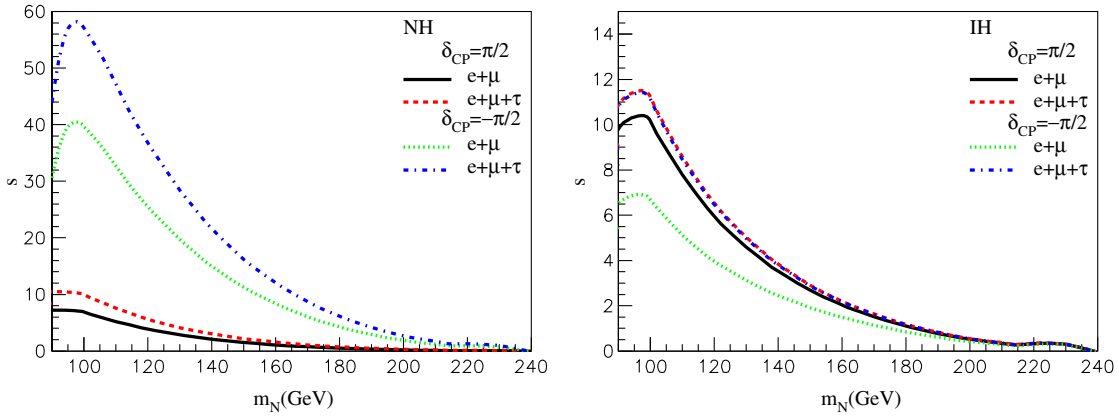

FIG. 10. The significance s vs m_N for NH (left) and IH (right) with integrated luminosity 5 ab^{-1}. We choose $e^y = 1750$, $\delta_{CP} = \pm\pi/2$, $\phi_1 = \phi_2 = \phi_3 = 0$ for NH (the largest eigenvalue of the matrix of neutrino Yukawa couplings is $0.00173 \times \sqrt{m_N}$), and $e^y = 350$, $\delta_{CP} = \pm\pi/2$, $\phi_1 = \phi_2 = \phi_3 = 0$ for IH (the largest eigenvalue of the matrix of neutrino Yukawa couplings is $0.000447 \times \sqrt{m_N}$).

(1.61∶1∶1.32) for $\delta_{CP} = \pi/2$ ($\delta_{CP} = -\pi/2$). In the case of NH with $\delta_{CP} = -\pi/2$ and the case of IH with $\delta_{CP} = \pm\pi/2$, the three $|R_{lN}|$ are of similar magnitude, so $|R_{\mu N}|$ can be probed to order of 10^{-3} for 5 ab^{-1} with an enhanced production rate due to large $|R_{eN}|$. In the case of NH with $\delta_{CP} = \pi/2$, $|R_{eN}|$ is almost 10 times smaller than $|R_{\mu N}|$, then the mixing $|R_{\mu N}|$ of order of 10^{-2} can be probed for 5 ab^{-1}, which is similar to the case with a single nonzero $|R_{\mu N}|$ as given in Fig. 6.

To conclude, in the low energy seesaw model, due to the correlation of three different R_{lN}, sizable $|R_{eN}|$ leads to t-channel production of heavy sterile neutrinos and can give rise to a quite large total production cross section of $e^+e^- \to N\nu$ process. The $N \to ljj$ events, on the other

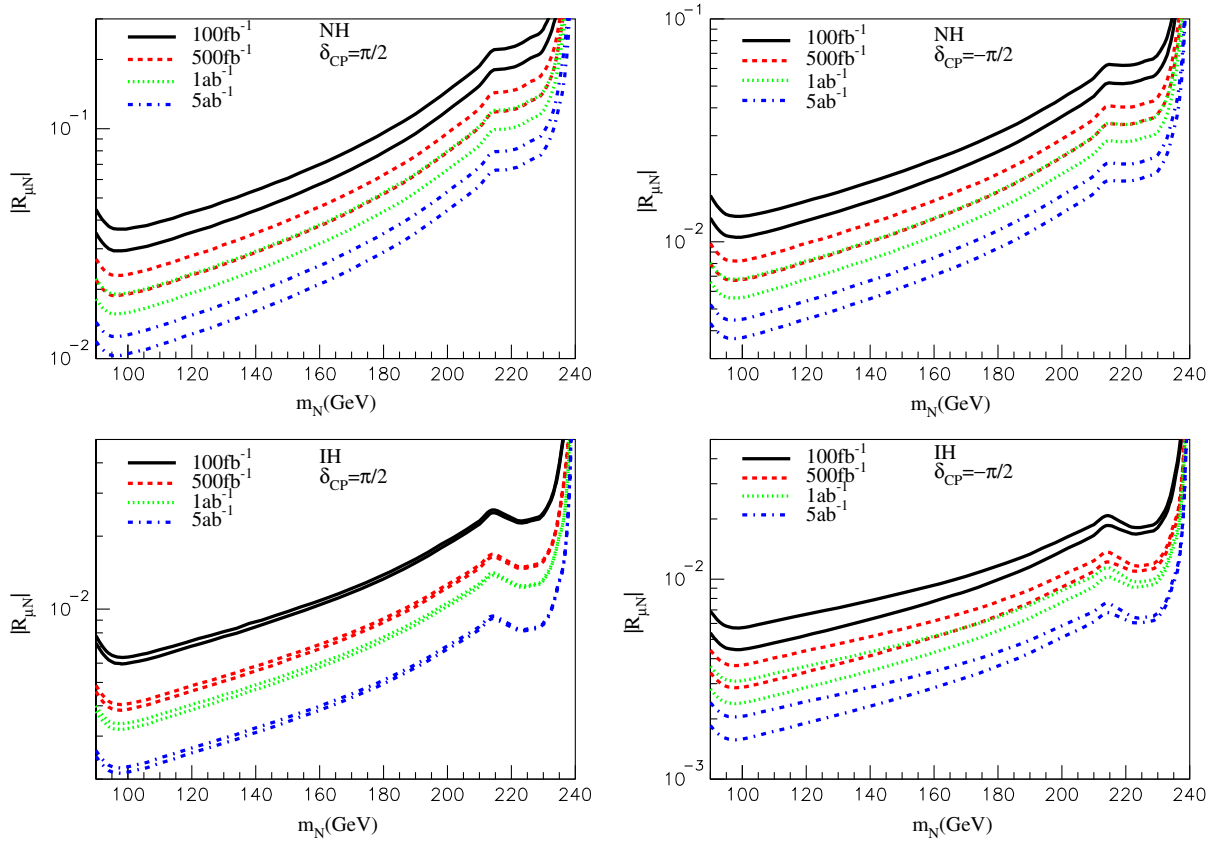

FIG. 11. Sensitivity to $|R_{\mu N}|$ with significance $s = 5$ for the cases of NH and IH and Dirac phase $\delta_{CP} = \pm\pi/2$, $\phi_1 = \phi_2 = \phi_3 = 0$. The curves of different type in each plot from up to down correspond to integrated luminosities 100 fb^{-1}, 500 fb^{-1}, 1 ab^{-1} and 5 ab^{-1}. The upper (lower) curve of the same type corresponds to $e + \mu$ ($e + \mu + \tau$) significances in each plot, respectively.

hand, can be dominated by μjj and τjj events because $|R_{\mu N}|^2 + |R_{\tau N}|^2$ can be much larger than $|R_{eN}|^2$ as can be seen in Fig. 1. For NH, in particular, $|R_{\mu N}|^2 + |R_{\tau N}|^2$ is always much larger than $|R_{eN}|^2$. In this case, $e + \mu$ significance and $e + \mu + \tau$ significance can be quite different, as can be seen in the left panel of Fig. 8. On the other hand, for IH, $|R_{\mu N}|^2 + |R_{\tau N}|^2$ can be of similar size of $|R_{eN}|^2$ and even much smaller than $|R_{eN}|^2$. In this case, the $e + \mu$ significance and $e + \mu + \tau$ significance would not be very different. This is the case for the right panel in Fig. 8. So analyzing the dominating of the N decay channel and the difference between the $e + \mu$ and $e + \mu + \tau$ significances can give hints regarding the mass hierarchy of neutrinos. In particular, if the dominating $N \to ljj$ events are ejj events, it has to be IH.

VI. CONCLUSION

In summary, we have studied the production, decay, and signature in ljj events of heavy Majorana-type sterile neutrinos of mass around 100 GeV at future CEPC. We study the tree-level decay of heavy sterile neutrinos by carefully taking into account the propagator of bosons, such as W and Z. Effects of on-shell and off-shell W and Z bosons are all taken into account by including the width of W and Z in the propagators. We obtain an analytic formula for tree-level decay of heavy sterile neutrinos which is valid for mass from tens of GeV to hundreds of GeV and higher energy. The formula is valid, in particular, for mass m_N around the masses of bosons.

For convenience and for later discussion in the low energy seesaw model of heavy sterile neutrinos, we have first studied the production of a single heavy sterile neutrino at CEPC and its signature. Although the mixing of a single heavy sterile neutrino with active neutrinos is strongly constrained by the $0\nu\beta\beta$ experiment, the study of the signature of a single heavy sterile neutrino is also of interests in and of itself, since some other particles or mechanisms, e.g., extra scalars or type-II seesaw, may exist to ease the constraint. We have shown that for a single heavy sterile neutrino, an electron positron collider such as CEPC is more sensitive to the mixing of a heavy sterile neutrino with electron (anti)neutrinos, than the mixing with muon or tau (anti)neutrinos. For the former, the production of N is associated with the production of an electron neutrino or antineutrino and can go through the t-channel. The cross section of the t-channel process can be two orders of magnitude larger than the cross section of the s-channel process which is responsible for probing the magnitude of the mixing with muon or tau (anti)neutrinos. We found that for an integrated luminosity 5 ab^{-1}, CEPC can reach a 5σ sensitivity of R_{eN}, the mixing of the sterile neutrino with active neutrinos, to a value as small as $|R_{eN}| = 10^{-3}$. For the mixing with muon and tau (anti)neutrinos $R_{\mu N}$ and $R_{\tau N}$, the 5σ sensitivity can reach $|R_{\mu N,\tau N}| \approx 10^{-2}$.

We also study the production of heavy sterile neutrinos in a low energy seesaw model and their signature at CEPC. In this model, two heavy sterile neutrinos exist so that an explanation of the masses and mixings of active neutrinos is available using the seesaw mechanism. In this model, the mixings of these two heavy sterile neutrinos with active neutrinos, R_{lN_1} and R_{lN_2}, are forced to have the same magnitude for all l, if we want these mixings to be large. In this case, the masses of these two sterile neutrinos are found to be degenerate or quasidegenerate if taking into account the constraint from the $0\nu\beta\beta$ experiment.

Therefore, the signature of these two heavy sterile neutrinos is just the double of the signature of a single heavy sterile neutrino discussed above. The major difference compared with the case of a single heavy sterile neutrino is that the mixing R_{lN_1} is no longer arbitrary for different l. Instead, values of R_{lN_1} for different l have some correlations. We take these facts into account. We find that the Dirac CP phase δ_{CP} in the PMNS mixing matrix of active neutrinos and Majorana phases affects the mixing R_{lN}, and changes the relative significance of ejj, μjj, and τjj events. Thus, a search for all 3 lepton channels is helpful to constrain the model. With sizable R_{eN}, the significance of both μ and τ channels will be enhanced, and will further constrain $R_{\mu N}$ and $R_{\tau N}$ compared to the case with only a single mixing.

We further note that although our analysis is for CEPC running at 240 GeV, it can also be applied to ILC running at around 250 GeV without much modification [43].

ACKNOWLEDGMENTS

This research is supported in part by the Natural Science Foundation of China (NSFC), Grants No. 11135009 and No. 11375065, and in part by the Shanghai Key Laboratory of Particle Physics and Cosmology, Grant No. 15DZ2272100. X. H. W. would like to thank Qi-Shu Yan for helpful discussions on MadGraph and CEPC.

APPENDIX: HEAVY STERILE NEUTRINO DECAYS

In this section we summarize the tree-level decay rate of sterile neutrinos decaying to three final fermions through interaction with the Z and W bosons induced by mixing with active neutrinos. Effects of on-shell and off-shell Z and W bosons are all taken into account by including the width of W and Z in the propagators. For example, for $N \to l_1^- l_2^+ \nu_{l_2}$ and $l_1 \neq l_2$, the decay rate is obtained as follows:

$$\Gamma(N \to l_1^- l_2^+ \nu_{l_2}) = |R_{l_1 N}|^2 \frac{G_F^2 m_N}{\pi^3} \int_0^{\frac{m_N}{2}} dE_1 \int_{\frac{m_N}{2}-E_1}^{\frac{m_N}{2}} dE_2 |X_W|^2 \times \frac{1}{2}(m_N - 2E_2)E_2, \tag{A1}$$

where X_W comes from the propagator of the W boson and is

$$X_W = \frac{m_W^2}{q^2 - m_W^2 + i\Gamma_W m_W}, \tag{A2}$$

where $q^2 = m_N^2 - 2m_N E_1$ and Γ_W is the total decay rate of W. $q = p - p_1$ is the four-momentum of the W boson where p and p_1 are the four-momenta of N and l_1, respectively. Thus, $q^2 = m_N^2 - 2m_N E_1$ when considering the decay of N at rest and neglecting the mass of l_1 with E_1 the energy of l_1. After performing integration in (A1), we can get a formula for the decay rate as a function of m_N, m_W, and Γ_W. Similarly, we can get formulas for other decays through Z boson exchange.

In the following we summarize the results:

(1) For $N \to l_1^- l_2^+ \nu_{l_2}$, $N \to l_1^+ l_2^- \bar{\nu}_{l_2}$ and $l_1 \neq l_2$

$$\Gamma(N \to l_1^- l_2^+ \nu_{l_2}) = \Gamma(N \to l_1^+ l_2^- \bar{\nu}_{l_2}) = |R_{l_1 N}|^2 \frac{G_F^2 m_N^5}{\pi^3} F_N(m_N, m_W, \Gamma_W), \tag{A3}$$

where F_N is a dimensionless function and is given in (A13) below.

(2) For $N \to l^- q_1 \bar{q}_2$, $N \to l^+ \bar{q}_1 q_2$

$$\Gamma(N \to l^- q_1 \bar{q}_2) = \Gamma(N \to l^+ \bar{q}_1 q_2) = |R_{lN}|^2 \frac{G_F^2 m_N^5}{\pi^3} N_C F_N(m_N, m_W, \Gamma_W) |K_{q_1 q_2}|^2. \tag{A4}$$

$K_{q_1 q_2}$ is the CKM matrix element in (q_1, q_2) entry, and $N_C = 3$ the number of color degrees of freedom of quarks.

(3) For $N \to l^- l^+ \nu_l$, $N \to l^+ l^- \bar{\nu}_l$

$$\begin{aligned}\Gamma(N \to l^- l^+ \nu_l) &= \Gamma(N \to l^+ l^- \bar{\nu}_l) \\ &= |R_{lN}|^2 \frac{G_F^2 m_N^5}{\pi^3} [F_N(m_N, m_W, \Gamma_W) + (C_L^2 + C_R^2) F_N(m_N, m_Z, \Gamma_Z) \\ &\quad + 2C_L F_S(m_N, m_W, \Gamma_W, m_Z, \Gamma_Z)],\end{aligned} \tag{A5}$$

where $C_{L,R}$ is given in (A10), F_S is a dimensionless function and is given below in (A15).

(4) For $N \to \nu_l \bar{l}' l'$ and $N \to \bar{\nu}_l l' \bar{l}'$

$$\Gamma(N \to \nu_l \bar{l}' l') = \Gamma(N \to \bar{\nu}_l l' \bar{l}') = |R_{lN}|^2 \frac{G_F^2 m_N^5}{\pi^3} (C_L^2 + C_R^2) F_N(m_N, m_Z, \Gamma_Z). \tag{A6}$$

(5) For $N \to \nu_l q \bar{q}$ and $N \to \bar{\nu}_l \bar{q} q$

$$\Gamma(N \to \nu_l \bar{l}' l') = \Gamma(N \to \bar{\nu}_l l' \bar{l}') = |R_{lN}|^2 \frac{G_F^2 m_N^5}{\pi^3} N_C [(C_L^q)^2 + (C_R^q)^2] F_N(m_N, m_Z, \Gamma_Z), \tag{A7}$$

where $q = u, d, c, s, b$ for $m_N < 2m_t$ and $C_{L,R}^q$ is given in (A11) and (A12).

(6) For $N \to \nu_l \nu_{l'} \bar{\nu}_{l'}$ and $N \to \bar{\nu}_l \bar{\nu}_{l'} \nu_{l'}$, $l \neq l'$

$$\Gamma(N \to \nu_l \nu_{l'} \bar{\nu}_{l'}) = \Gamma(N \to \bar{\nu}_l \nu_{l'} \bar{\nu}_{l'}) = |R_{lN}|^2 \frac{G_F^2 m_N^5}{\pi^3} C_\nu^2 F_N(m_N, m_Z, \Gamma_Z), \tag{A8}$$

where $C_\nu = 1/2$.

(7) For $N \to \nu_l \nu_l \bar{\nu}_l$ and $N \to \bar{\nu}_l \bar{\nu}_l \nu_l$

$$\Gamma(N \to \nu_l \nu_l \bar{\nu}_l) = \Gamma(N \to \bar{\nu}_l \nu_l \bar{\nu}_l) = |R_{lN}|^2 \frac{G_F^2 m_N^5}{\pi^3} 4C_\nu^2 F_N(m_N, m_Z, \Gamma_Z). \tag{A9}$$

Couplings C_L, C_R, etc. which appear in expressions above, are given as

$$C_L = -\frac{1}{2} + \sin^2\theta_W, \qquad C_R = \sin^2\theta_W, \tag{A10}$$

$$C_L^u = \frac{1}{2} - \frac{2}{3}\sin^2\theta_W, \qquad C_R^u = -\frac{2}{3}\sin^2\theta_W, \tag{A11}$$

$$C_L^u = -\frac{1}{2} + \frac{1}{3}\sin^2\theta_W, \qquad C_R^u = \frac{1}{3}\sin^2\theta_W. \tag{A12}$$

For mass m_N, m_X, and decay rate Γ_X, the function F_N used above is

$$\begin{aligned} F_N(m_N, m_X, \Gamma_X) = \frac{m_X^4}{96 m_N^8}\Bigg\{ & -2m_N^2(m_N^2 - m_X^2) \\ & + (A_X + C_X\Gamma_X^2 m_X^2)\frac{1}{\Gamma_X m_X}\left[\arctan\left(\frac{m_N^2 - m_X^2}{\Gamma_X m_X}\right) - \arctan\left(\frac{-m_X^2}{\Gamma_X m_X}\right)\right] \\ & - \frac{1}{2}(B_X + 2\Gamma_X^2 m_X^2)\ln\left(\frac{\Gamma_X^2 m_X^2 + (m_N^2 - m_X^2)^2}{\Gamma_X^2 m_X^2 + m_X^4}\right)\Bigg\} \end{aligned} \tag{A13}$$

where

$$A_X = (m_N^2 - m_X^2)^2(m_N^2 + 2m_X^2), \qquad B_X = 6(m_N^2 - m_X^2)m_X^2, \qquad C_X = 3(m_N^2 - 2m_X^2). \tag{A14}$$

Function F_S in (A5) is given as

$$F_S = \frac{1}{m_N^4}\int_0^{\frac{m_N}{2}} dE_1 \int_{\frac{m_N}{2}-E_1}^{\frac{m_N}{2}} dE_2 (X_W X_Z^* + X_W^* X_Z)\frac{1}{2}(m_N - 2E_2)E_2, \tag{A15}$$

where

$$X_Z = \frac{m_Z^2}{q_3^2 - m_Z^2 + i\Gamma_Z m_Z}. \tag{A16}$$

$q_3^2 = m_N^2 - 2m_N E_3$ with $E_3 = m_N - E_1 - E_2$ when considering the decay of N at rest and neglecting the mass of final fermions. Equation (A15) can not be obtained as an explicit function of m_N, m_W, and m_Z. We can calculate this function numerically.

For the $N \to \nu H$ decay, the effect described here can be similarly obtained with the introduction of a function $F_N(m_N, m_H, \Gamma_H)$. For example, for $N \to \nu_l \bar{f} f$ and $N \to \bar{\nu}_l \bar{f} f$

$$\Gamma(N \to \nu_l \bar{f} f) = \Gamma(N \to \bar{\nu}_l \bar{f} f) = \frac{g^2 m_N^7 |R_{lN}|^2 y_f^2}{16\pi^3 m_W^2 m_H^4} N_f F_N(m_N, m_H, \Gamma_H), \tag{A17}$$

where y_f is the Yukawa coupling of the fermion f, $N_f = 1$ for f being a lepton and $N_f = 3$ for f being a quark. Interference of the N decay through the Z boson and H boson vanishes. Since the Yukawa coupling to fermion f is always small for $f = b$, c, s, d, u and leptons, inclusion of N decay through the neutral Higgs boson does not change significantly the signature of the sterile neutrino N discussed in this article, as long as we are not going to concentrate on the signature of N coming from $N \to \nu_l b\bar{b}$ and $N \to \bar{\nu}_l b\bar{b}$ decay.

In the low energy limit $m_N^2 \ll m_W^2$, we have $|X_W| \approx |X_Z| \approx 1$, and the above equations of decay rate, (A3), (A4), (A5), (A6), (A7), (A8), (A9), can be simplified as follows:

(1) For $N \to l_1^- l_2^+ \nu_{l_2}$, $N \to l_1^+ l_2^- \bar{\nu}_{l_2}$, and $l_1 \neq l_2$

$$\Gamma(N \to l_1^- l_2^+ \nu_{l_2}) = \Gamma(N \to l_1^+ l_2^- \bar{\nu}_{l_2}) = |R_{l_1 N}|^2 \frac{G_F^2 m_N^5}{192\pi^3}, \tag{A18}$$

(2) For $N \to l^- q_1 \bar{q}_2$, $N \to l^+ \bar{q}_1 q_2$

$$\Gamma(N \to l^- q_1 \bar{q}_2) = \Gamma(N \to l^+ \bar{q}_1 q_2) = |R_{lN}|^2 \frac{G_F^2 m_N^5}{192\pi^3} N_C |K_{q_1 q_2}|^2. \tag{A19}$$

(3) For $N \to l^- l^+ \nu_l$, $N \to l^+ l^- \bar{\nu}_l$

$$\Gamma(N \to l^- l^+ \nu_l) = \Gamma(N \to l^+ l^- \bar{\nu}_l) = |R_{lN}|^2 \frac{G_F^2 m_N^5}{192\pi^3} [(1 + C_L)^2 + C_R^2], \tag{A20}$$

(4) For $N \to \nu_l \bar{l}' l'$ and $N \to \bar{\nu}_l l' \bar{l}'$

$$\Gamma(N \to \nu_l \bar{l}' l') = \Gamma(N \to \bar{\nu}_l l' \bar{l}') = |R_{lN}|^2 \frac{G_F^2 m_N^5}{192\pi^3} (C_L^2 + C_R^2). \tag{A21}$$

(5) For $N \to \nu_l q \bar{q}$ and $N \to \bar{\nu}_l \bar{q} q$

$$\Gamma(N \to \nu_l \bar{l}' l') = \Gamma(N \to \bar{\nu}_l l' \bar{l}') = |R_{lN}|^2 \frac{G_F^2 m_N^5}{192\pi^3} N_C [(C_L^q)^2 + (C_R^q)^2]. \tag{A22}$$

(6) For $N \to \nu_l \nu_{l'} \bar{\nu}_{l'}$ and $N \to \bar{\nu}_l \bar{\nu}_{l'} \nu_{l'}$, $l \neq l'$

$$\Gamma(N \to \nu_l \nu_{l'} \bar{\nu}_{l'}) = \Gamma(N \to \bar{\nu}_l \nu_{l'} \bar{\nu}_{l'}) = |R_{lN}|^2 \frac{G_F^2 m_N^5}{192\pi^3} C_\nu^2, \tag{A23}$$

(7) For $N \to \nu_l \nu_l \bar{\nu}_l$ and $N \to \bar{\nu}_l \bar{\nu}_l \nu_l$

$$\Gamma(N \to \nu_l \nu_l \bar{\nu}_l) = \Gamma(N \to \bar{\nu}_l \nu_l \bar{\nu}_l) = |R_{lN}|^2 \frac{G_F^2 m_N^5}{192\pi^3} 4 C_\nu^2. \tag{A24}$$

In all these results, the masses of the final fermions have all been neglected.

[1] P. Minkowski, Phys. Lett. B **67**, 421 (1977); T. Yanagida, in *Proceedings of the Workshop on the Unified Theory and the Baryon Number in the Universe*, edited by O. Sawada and A. Sugamoto (KEK Collaboration, Tsukuba, 1979), p. 95; M. Gell-Mann, P. Ramond, and R. Slansky, in *Supergravity*, edited by P. van Nieuwenhuizen and D. Freedman (North-Holland, Amsterdam, 1979), p. 315; S. L. Glashow, in *Proceedings of the 1979 Cargese Summer Institute on Quarks and Leptons*, edited by M. Levy *et al.* (Plenum Press, New York, 1980), p. 687; R. N. Mohapatra and G. Senjanovic, Phys. Rev. Lett. **44**, 912 (1980).

[2] T. Asaka and M. Shaposhnikov, Phys. Lett. B **620**, 17 (2005); T. Asaka, S. Blanchet, and M. Shaposhnikov, Phys. Lett. B **631**, 151 (2005).

[3] X.-G. He, T. Li, and W. Liao, Phys. Rev. D **81**, 033006 (2010).

[4] W. Liao, Phys. Rev. D **82**, 073001 (2010).

[5] M. Acciarri *et al.* (L3 Collaboration), Phys. Lett. B **461**, 397 (1999).

[6] P. Achard *et al.* (L3 Collaboration), Phys. Lett. B **517**, 67 (2001).

[7] F. del Aguila, E. Laermann, and P. M. Zerwas, Nucl. Phys. **B297**, 1 (1988).

[8] W. Buchmuller and C. Greub, Nucl. Phys. **B363**, 345 (1991).

[9] J. Gluza and M. Zralek, Phys. Rev. D **48**, 5093 (1993).

[10] A. Djouadi, Z. Phys. C **63**, 317 (1994).

[11] G. Azuelos and A. Djouadi, Z. Phys. C **63**, 327 (1994).

[12] R. Vuopionpera, Z. Phys. C **65**, 311 (1995).

[13] J. Gluza and M. Zralek, Phys. Lett. B **372**, 259 (1996).

[14] J. Gluza and M. Zralek, Phys. Rev. D **55**, 7030 (1997).

[15] A. Hofer and L. M. Sehgal, Phys. Rev. D **54**, 1944 (1996).

[16] J. Gluza, J. Maalampi, M. Raidal, and M. Zralek, Phys. Lett. B **407**, 45 (1997).

[17] G. Cvetic, C. S. Kim, and C. W. Kim, Phys. Rev. Lett. **82**, 4761 (1999).

[18] F. del Aguila, J. A. Aguilar-Saavedra, A. Martinez de la Ossa, and D. Meloni, Phys. Lett. B **613**, 170 (2005).

[19] A. Das and N. Okada, Phys. Rev. D **88**, 113001 (2013).

[20] A. Blondel *et al.* (FCC-ee study Team), Nucl. Part. Phys. Proc. **273–275**, 1883 (2016).

[21] S. Banerjee, P. S. B. Dev, A. Ibarra, T. Mandal, and M. Mitra, Phys. Rev. D **92**, 075002 (2015).
[22] A. Caputo, P. Hernandez, M. Kekic, J. López-Pavón, and J. Salvado, Eur. Phys. J. C **77**, 258 (2017).
[23] S. Antusch, E. Cazzato, and O. Fischer, J. High Energy Phys. 12 (2016) 007.
[24] S. Antusch, E. Cazzato, and O. Fischer, Int. J. Mod. Phys. A **32**, 1750078 (2017).
[25] S. S. Biswal and P. S. B. Dev, Phys. Rev. D **95**, 115031 (2017).
[26] C. X. Yue, Y. C. Guo, and Z. H. Zhao, Nucl. Phys. **B925**, 186 (2017).
[27] CEPC-SppC Preliminary Conceptual Design Report, http://cepc.ihep.ac.cn/preCDR/volume.html.
[28] P. Benes, A. Faessler, F. Simkovic, and S. Kovalenko, Phys. Rev. D **71**, 077901 (2005).
[29] K. A. Olive *et al.* (Particle Data Group), Chin. J. Phys. C **38**, 090001 (2014).
[30] S. Antusch, C. Biggio, E. Fernandez-Martinez, M. B. Gavela, and J. Lopez-Pavon, J. High Energy Phys. 10 (2006) 084.
[31] S. Antusch, J. P. Baumann, and E. Fernandez-Martinez, Nucl. Phys. **B810**, 369 (2009).
[32] A. Ibarra, E. Molinaro, and S. T. Petcov, Phys. Rev. D **84**, 013005 (2011).
[33] M. Drewes and B. Garbrecht, Nucl. Phys. **B921**, 250 (2017).
[34] A. de Gouva and A. Kobach, Phys. Rev. D **93**, 033005 (2016).
[35] E. Fernandez-Martinez, J. Hernandez-Garcia, and J. Lopez-Pavon, J. High Energy Phys. 08 (2016) 033.
[36] J. Alwall, R. Frederix, S. Frixione, V. Hirschi, F. Maltoni, O. Mattelaer, H.-S. Shao, T. Stelzer, P. Torrielli, and M. Zaro, J. High Energy Phys. 07 (2014) 079.
[37] A. Alloul, N. D. Christensen, C. Degrande, C. Duhr, and B. Fuks, Comput. Phys. Commun. **185**, 2250 (2014).
[38] C. Degrande, C. Duhr, B. Fuks, D. Grellscheid, O. Mattelaer, and T. Reiter, Comput. Phys. Commun. **183**, 1201 (2012).
[39] A. Atre, T. Han, S. Pascoli, and B. Zhang, J. High Energy Phys. 05 (2009) 030.
[40] F. del Aguila and J. A. Aguilar-Saavedra, Nucl. Phys. **B813**, 22 (2009).
[41] T. Sjostrand, S. Mrenna, and P. Z. Skands, J. High Energy Phys. 05 (2006) 026.
[42] J. Conway, Pretty Good Simulator webpage, http://conway.physics.ucdavis.edu/research/software/pgs/pgs4-general.htm.
[43] K. Fujii *et al.*, arXiv:1710.07621.